OPEN ACCESS
Journal of Innovative Optical Health Sciences
Vol. 14, No. 1 (2021) 2140003 (7 pages)

DOI: 10.1142/S1793545821400034

World Scientific
www.worldscientific.com

A method of removing retardance induced by scattering of collagenous fiber bundles

Wanrong Gao* and Siyu Liu
Department of Optical Engineering
Nanjing University of Science and Technology
200 Xiao Ling Wei, Nanjing, Jiangsu 210094, P. R. China
**wgao@njust.edu.cn*

Received 9 September 2020
Accepted 24 November 2020
Published 16 December 2020

In this work, we report a method of removing scattering induced retardance in polarization sensitive full field optical coherence tomography (PS-FFOCT). First, the Mueller matrix that describes its operation is derived. The thickness invariant retardance induced by the scattering of collagenous fiber bundles is then used to find the accurate values of the birefringence of the layers that consist collagenous fibers. Finally, the initial *en face* birefringent images of *in vitro* beef tendon samples are presented to demonstrate the capability of our method.

Keywords: Mueller matrix polarimeter; birefringent structures; collagenous fibers.

1. Introduction

Polarization parameters can be used to quantify various types of anisotropic structures. Several techniques are possible for obtaining polarization parameters of a medium. The direct consequences of the polarization effects of the medium are to modify the polarization states of the polarized light incident on the sample surface and backscattered from it. So a simple way of measuring the polarization properties of a medium is to observe the changes in polarization state of backscattered with as a function of the depth. For example, for the birefringent medium, the changes are directly related to the phase retardation induced by anisotropic structures of tissue from sample surface to the depth which is the result of birefringence.[1] The presence of phase retardation in the phase retardation image suggests the existence of birefringent tissues or the existence of birefringence appears as increase in the cumulative phase retardation with the depth for homogeneous birefringent media.

Real tissues are optically anisotropic and often have several types of polarization properties simultaneously such as linear birefringence and linear diattenuation along the x–y axes. The Jones matrix formalism is then used to analyze the measurements.[2] However, birefringent tissues are not uniformly distributed in real tissues. For example, the orientation of the optic axis may vary in depth. Thus the cumulative phase retardation derived from the measured Jones matrix is not an accurate representation of the birefringent structures. Local

Jones matrix of a thin layer of tissue was then proposed.[3–6] Note that the Jones matrix of a thin layer is proportional to the derivative of the cumulative Mueller matrix of the tissue from the surface to the depth. In addition, for a weakly birefringent tissue and a thin slice of tissue, the resulted phase retardation is expected to be very small. Thus, this reconstruction method is susceptible to measurement noises.

To improve the accuracy of the measured polarization parameters, averaging over the Jones matrices between adjacent pixels will be beneficial. However, spatial averaging over the Jones matrices of adjacent pixels requires special attention to adjust the global phase between the Jones matrices of adjacent pixels to avoid unwanted interference effects.[6–8] To solve this problem, the Mueller matrix formalism has been employed because the Mueller matrix is defined in terms of the intensity-based quantities of the light. In fact, this idea has been used to overcome the limitation of the coherent Jones matrix by Villiger *et al.*[9] The incoherent spatial average of the Mueller matrices adjacent pixels along the depth direction was first calculated to remove the speckle noises and the depth-resolved local tissue birefringence was then extracted from the averaged Mueller matrix, removing the global phase value that creates interference effects in the Jones matrices of adjacent pixels.

In the past several decades, several types of OCT-based polarimetric configurations have been proposed that measure the birefringence,[10] orientation of optic axis,[11] diattenuation,[12] and depolarization[13] of an anisotropic sample. Most of these schemes mainly consist of a light beam scanning PS-OCT and the Jones matrices are employed to represent the polarization properties of the optical elements and the samples. Although a Mueller matrix beam scanning PS-OCT setup was proposed only the images of 16 elements of the Mueller matrix were presented and the images of polarization properties such as birefringence were not given.[14,15]

Full-field optical coherence tomography (FFOCT) instruments can generate tomographic *en-face* images of live tissues or tissue samples with a spatial resolution of $\sim 1\,\mu$m in three dimension.[16–19] When polarization-sensitive measurement part is added in the conventional light intensity detection FFOCT system, the so-called polarization sensitive FFOCT (PS-FFOCT) can give depth-resolved *en-face* images of polarization properties such as birefringence and orientation of optic axis at a depth beneath tissue surface.[20–23]

Note that for the imaging of biological tissues at a specific depth beneath the surface with OCT-based instruments, several important effects limit the final image quality. One is the aberrations induced by overlying layers of tissue structures. Second, because the light experiences multiple scattering still has some temporal and spatial coherence, the speckles are induced by multiply scattered light. For FFOCT, because it has resolution in both lateral and depth (axial) directions at the level of $\sim 1\,\mu$m these two effects become more significant. In addition, it has been shown theoretically that in the reflection measurement of birefringent tissues consisting of fiber bundles the total retardance is the sum of the retardance due to the birefringence of the fiber bundles layer, which is proportional to the thickness, and the retardance due to the fiber scattering, which is thickness invariant.[24] It is then desirable to identify and remove the retardance induced by the scattering of collagenous fiber bundles in order to correctly interpret the birefringence of the tissue and obtain the information about the spatial organization of collagenous fiber bundles.

In this work, we describe a Mueller matrix polarization sensitive full field optical coherence tomography (PS-FFOCT) setup which mainly consists of a Linnik microscopic interferometer and a polarization detection device. In the analysis of the system performance, Mueller matrices are used to represent the polarization properties of the optical elements and the samples. In order to obtain the accurate values of the birefringence of the fiber bundles layer, the scattering Mueller matrix of sample surface is used to remove the retardance due to the fiber scattering.

2. Theory

As mentioned above, although FFOCT has a high spatial resolution in three dimensions ($\sim 1\,\mu$m), PS-FFOCT measures the round-trip Jones matrix or Mueller matrix. In order to calculate the local polarization properties of medium in which the orientation of optic axis varies in depth (for example), first the expression for the Mueller matrix of a thin sample layer at a given depth is considered.

The incident polarized light propagates through overlying layers, is backscattered from a thin layer

with a thickness Δz at the depth z, and passes through the sample from the depth z to the sample surface. Note that the same fiber structures contribute to both the form birefringence and light scattering. Although OCT technique can measure the light only backscattered from a thin layer at a given sample depth change in the state of polarization of the measured light is due to the cumulative effects of the Mueller matrices of the polarization elements and the layers of the sample overlying the thin slice of the medium to be imaged.

At a pixel on the detector, the Mueller matrix $\mathbf{M}(z)$ of the transmission to a thin layer at the depth z and back to the detector can be expressed as

$$\mathbf{M}(z) = \mathbf{M}_{\text{det}}(\mathbf{M}_{\text{rev}}\mathbf{M}_s\mathbf{M}_{\text{for}})\mathbf{M}_{\text{ill}}, \tag{1}$$

where $\mathbf{M}_{\text{ill}}$ is the Mueller matrix of the polarization elements from the polarizer in the illumination path to the sample surface, and $\mathbf{M}_{\text{det}}$ is the Mueller matrix of the polarization elements from the sample surface to the detector, $\mathbf{M}_s$ is the Mueller matrix formed by incoherent summation of the scattering matrices of the structures in the thin slice,[24,25] $\mathbf{M}_{\text{for}}$ and $\mathbf{M}_{\text{rev}}$ are Mueller matrices of the overlying medium for the incident and reflected light traversing the layers of medium to the depth z. Here, each pixel on the detector images a finite transverse section of the sample and pixels are independent as a consequence of the spatially incoherent thermal light illumination.

In the backscattered case, $\mathbf{M}_{\text{rev}} = \mathbf{D}\mathbf{M}_{\text{for}}^T\mathbf{D}$, where $\mathbf{D} = \text{diag}(1, 1, 1, -1)$ is a diagonal matrix, and the superscript T stands for transposition. We then have

$$\mathbf{M}(z) = \mathbf{M}_{\text{det}}[(\mathbf{D}\mathbf{M}_{\text{for}}^T\mathbf{D})\mathbf{M}_s\mathbf{M}_{\text{for}}]\mathbf{M}_{\text{ill}}. \tag{2}$$

Note that tissue polarization properties mainly arise from their directional fibrous organization. For example, the polarization properties of human skin are due to its dense collagenous fiber bundles for human skin[6] and the nerve fiber layer in human retina is the source of its birefringence and diattenuation.[26] Based on these facts, the fiber structures can be modeled as a weakly reflecting array of approximately parallel, nonabsorbing, dielectric cylinders.[24] The Mueller matrix $\mathbf{M}_s$ is then the summation of the scattering Mueller matrix of each cylinder in the thin layer of the thickness Δz and is evidently dependent on the spatial distribution of the arrays of fibers. Compared with fiber-optic imaging probes in which the single mode fiber induces the random birefringence,[27] our PS-FFOCT is a free space system with bulk optics. So, both $\mathbf{M}_{\text{ill}}$ and $\mathbf{M}_{\text{det}}$ are pure retarders and their forms are known.

To determine $\mathbf{M}_s$ we first measure the transmission Mueller matrix $\mathbf{M}(0)$ of the optical path from linear polarizer to the sample surface and from there to the detector. In this case, the corresponding Mueller matrix at each point in the image is given by

$$\mathbf{M}(0) = \mathbf{M}_{\text{det}}\mathbf{M}_s\mathbf{M}_{\text{ill}}. \tag{3}$$

From Eq. (3), we have

$$\mathbf{M}_s = \mathbf{M}_{\text{det}}^{-1}\mathbf{M}(0)\mathbf{M}_{\text{ill}}^{-1}, \tag{4}$$

where the superscript "-1" denotes the inverse of the matrix. Note the fact that the scattering matrix is thickness invariant,[24] a combination of Eqs. (2) and (4) then allows us to determine the form of $\mathbf{M}_{\text{for}}$.

Note that $\mathbf{M}_{\text{for}}$ contains the cumulative retardation from the sample surface to a given depth within medium. So, the model is valid for the medium with its orientation of the optic axis is depth invariant. Because Mueller matrix contains all the polarization properties of the medium Eqs. (1)–(4) can be used to derive any type of polarization parameter of the medium.[1,28]

Note that the diattenuation of biological tissues reported is much smaller than the birefringence of the investigated samples.[29–31] Assuming that diattenuation is very small and is negligible, the overlying layer acts as an ideal homogeneous linear retarder with its slow axis parallel to the cylinders. The Mueller matrix $\mathbf{M}_{\text{for}}$ for a linear retarder with retardance δ and with its slow axis at an angle θ of rotation with respect to the horizontal axis is then of the form[32]:

$$\mathbf{M}_{\text{for}}(\delta, \theta) = \begin{pmatrix} 1 & 0 & 0 & 0 \\ 0 & \cos^2(2\theta) + \sin^2(2\theta)\cos\delta & \sin(2\theta)\cos(2\theta)(1 - \cos(\delta)) & -\sin(2\theta)\sin\delta \\ 0 & \sin(2\theta)\cos(2\theta)(1 - \cos(\delta)) & \sin^2(2\theta) + \cos^2(2\theta)\cos\delta & \cos(2\theta)\sin(\delta) \\ 0 & \sin(2\theta)\sin\delta & -\cos(2\theta)\sin(\delta) & \cos(\delta) \end{pmatrix}, \tag{5}$$

where $\delta = 2\pi z \Delta n/\lambda_c$, Δn is the birefringence of the medium, λ_c is the center wavelength. In the case when the slow axis is parallel to the horizontal axis, Eq. (5) reduces to

$$\mathbf{M}_{\text{for}}(\delta) = \begin{pmatrix} 1 & 0 & 0 & 0 \\ 0 & 1 & 0 & 0 \\ 0 & 0 & \cos\delta & \sin(\delta) \\ 0 & 0 & -\sin(\delta) & \cos\delta \end{pmatrix}. \quad (6)$$

Equations (5) and (6) can be employed to calculate the birefringence and the orientation of optic axis from measured Mueller matrix.

3. Experimental Configuration

As can be seen from Eq. (1) to measure the Mueller matrix, the polarization elements in the illumination path in the setup must generate at least four linearly independent polarization states represented by incident Stokes vectors. The corresponding polarization states represented by output Stokes vectors of light backscattered from within the sample are measured by polarization analyzing elements and detectors. However, in this initial experiment, we only consider the measurements of the magnitude of birefringence of the sample.

Consider the general polarimetric arrangement of a PS-FFOCT setup shown in Fig. 1. The details of the setup are described in Ref. 23. Briefly, it mainly consists of Linnik interference microscope combined with a low coherence illumination from a tungsten halogen lamp and polariemtric measurement.

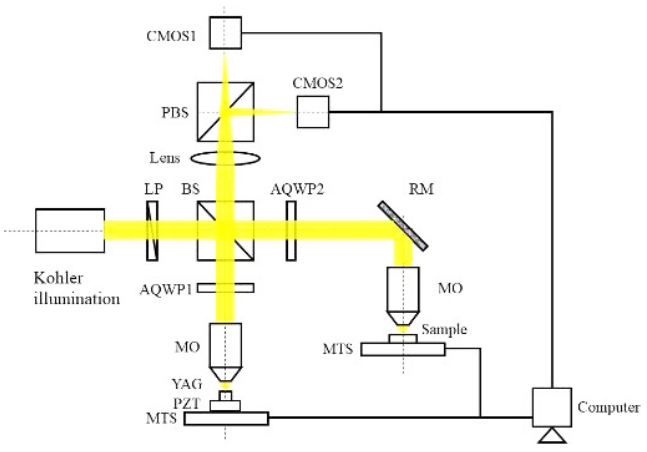

Fig. 1. Schematic of the PS-FFOCT system. LP: linear polarization: BS: beam splitter; PBS: polarization beam splitter; AQWP: achromatic quarter-wave plate; MO: microscope objective; MTS: motorized translation stage.

The system is illuminated by a 150-W tungsten halogen lamp with a center wavelength of 563 nm, and a bandwidth of 150 nm (HLX, Osram). The light is polarized along the horizontal direction $\hat{x}$ by linear polarizer (LP) and then is split into the reference and sample arms by a nonpolarizing beam splitter cube (BS). An achromatic quarter-wave plate 1 (AQWP1) is placed in the reference arm with the slow axis oriented at a 22.5° from the horizontal direction $\hat{x}$. So, the light reflected from the reference mirror undergoes a round trip half-wave shift and returns with a linear polarization at 45° from the horizontal direction, providing equal reference beam power in the two orthogonal detection channels in the detection arm. A quarter-wave plate (AQWP2) oriented at 45° from the horizontal direction $\hat{x}$ is placed in the sample arm to provide a circularly polarized illumination on the sample. The light backscattered from within the sample is superposed with the light reflected from the reference by the BS.

The superposed light is then split into two orthogonal components by the polarization beam splitter (PBS) and measured by COMS1 and COMS2 (MV1-D1024E-160 _CL, Photonfocus) with pixel matrix size of 1024×1024 simultaneously, along the detection axes $\hat{x}$ (parallel to the incident polarization) and $\hat{y}$ (perpendicular to the incident polarization), respectively. The polished surface of a YAG (Y3Al5O12) crystal rod acts as a reflecting mirror in the reference arm of the interferometer. A piezoelectric transducer (PZT) (AE0505D18F, Thorlabs) stage is employed to generate a sinusoidal modulation in the interference signals. Note that the YAG crystal was attached to a PZT. Our FFOCT setup has a lateral resolution of 0.98 μm and an axial resolution of 2.4 μm, respectively.

The *in vitro* beef tendon samples were imaged with our PS-FFOCT setup. This study was approved by the Ethics Committee of Nanjing University of Science and Technology and in accord with the institutional policy to protect the animals.

4. Results

In our PS-FFOCT system, two two-dimensional array cameras are employed to detect the horizontally polarized and vertically polarized components of the interference signals. In our experiments, a

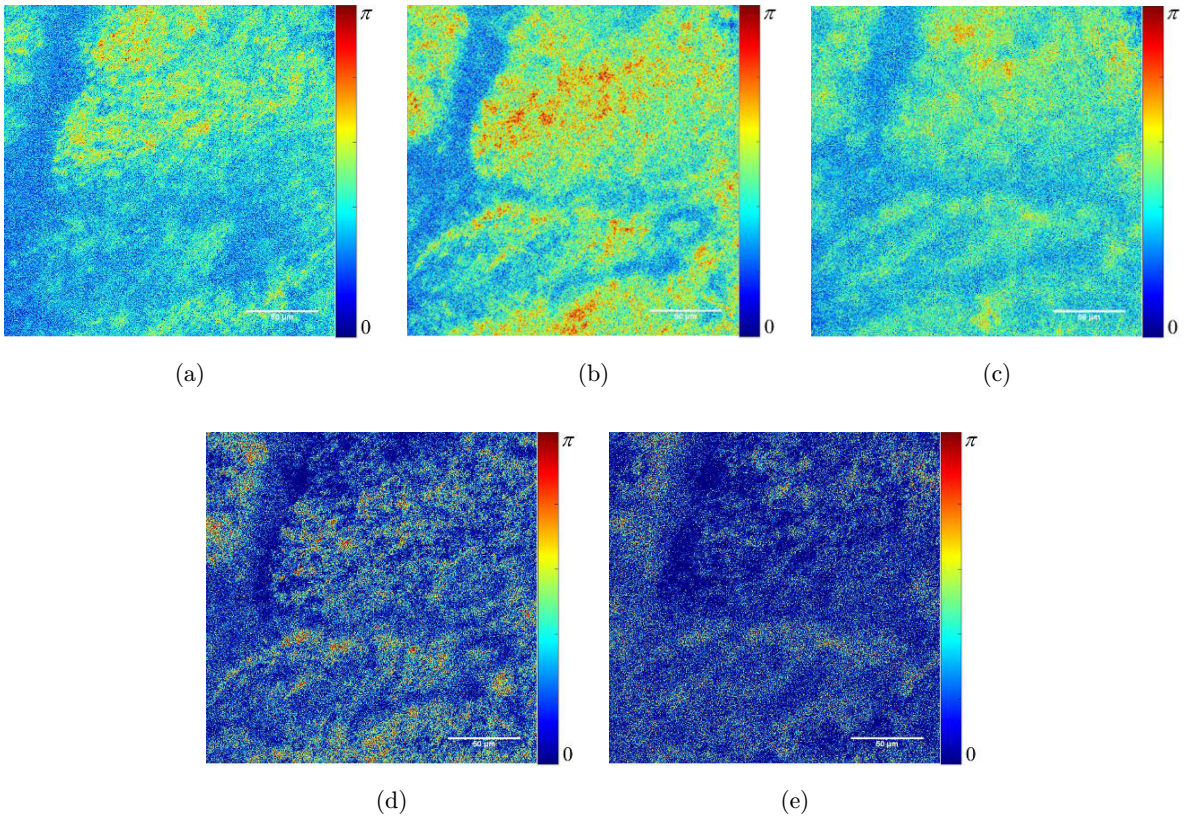

Fig. 2. *En-face* images of *in vitro* beef tendon. (a) *En-face* image of surface scattering-induced phase-retardation image; (b), (c) *en-face* images of linear birefringence-induced images at depths of 10 μm and 20 μm, respectively; (d) and (e) *en-face* images of linear birefringence-induced images at depths of 10 μm and 20 μm, respectively, obtained by subtracting surface scattering-induced phase-retardation. The scale bar is 50 μm.

sinusoidal modulation method is used to calculate the intensity and phase retardation with our PS-FFOCT setup.[23] As mentioned above, by using the fact that the scattering matrix $\mathbf{M}_s$ is thickness invariant (see Eqs. (3) and (4)), the accurate values of the cumulative retardation from the sample surface to a given depth within medium contained in $\mathbf{M}_{\text{for}}$ can be obtained by subtracting the surface scattering-induced phase-retardation.

Figure 2 shows the *en-face* images of *in vitro* beef tendon. Figure 2(a) presents *en-face* image of surface scattering-induced phase-retardation image, Figs. 2(b) and 2(c) depict *en-face* images of linear birefringence-induced images at depths of 10 μm and 20 μm, respectively, and Figs. 2(d) and 2(e) are *en-face* images of linear birefringence-induced images at depths of 10 μm and 20 μm obtained by subtracting surface scattering-induced phase-retardation. Note that the surface scattering-induced phase-retardance is not uniform due to the rough sample surface. The change of the birefringent structures with depth can be seen clearly from Figs. 2(b)–2(e), respectively. A comparison of the lower part of each image in Fig. 2 reveals that, in this region, the contribution to the phase-retardation is mainly due to the birefringence of the layer as the scattering-induced phase-retardation is very low. In addition, in the regions where the scattering-induced phase-retardation is strong such as the upper region of the image, the subtraction operation allows the correct interpretation of the measured phase retardance.

5. Discussions

It should be pointed out that the light reflected from the sample surface has been measured by other authors.[27] In their work, the Jones matrices of optical path to the surface and reflected from there have been used to remove birefringence induced by fiber-optic components in the optical paths in the Jones formalism. In addition, a Jones matrix

representation of the PS-FFOCT has been reported.[21,22] However, in their analysis, they focused on the birefringence induced by the defects inside multiplayer optical coatings. Our analysis is based on the fact that the retardance induced by cylindrical scattering is depth in variant. In addition, collagenous fibers in real human tissue samples are assumed to randomly distributed. So, the Mueller matrix of a thin layer of the collagenous fibers can be obtained by incoherent summing of the scattering matrices of the cylinder in the layer.

Compared with the Jones matrix method, incoherent spatial averaging over Mueller matrices of adjacent pixels can be calculated to suppress the speckle noise. Note that our method can also be employed to derive the information about the collagenous fibers in real human tissues from measured Mueller matrix of a thin layer of the medium at the sample surface. This is possible because the Mueller matrix of the thin layer of collagenous fibers can be expressed as[24,25]

$$\mathbf{M}_s = \begin{pmatrix} m_{s11} & m_{s12} & 0 & 0 \\ m_{s12} & m_{s11} & 0 & 0 \\ 0 & 0 & m_{s33} & -m_{s34} \\ 0 & 0 & m_{s34} & m_{s33} \end{pmatrix}, \quad (7)$$

where

$$m_{s11} = \frac{1}{2}(p_1 + p_2), \quad m_{s12} = \frac{1}{2}(p_1 - p_2),$$
$$m_{s33} = \rho\cos(\Delta_s), \quad m_{s34} = \rho\sin(\Delta_s), \quad (8a)$$
$$p_1 = \sum_{c=1}^{n} \rho_{c1}^2, \quad p_2 = \sum_{c=1}^{n} \rho_{c2}^2, \quad (8b)$$
$$\rho\cos(\Delta_s) = \sum_{c=1}^{n} \rho_{c1}\rho_{c2}\cos(\delta_c),$$
$$\rho\sin(\Delta_s) = \sum_{c=1}^{n} \rho_{c1}\rho_{c2}\sin(\delta_c), \quad (8c)$$

where ρ_{c1} and ρ_{c2} are the ratios of scattered-to-incident amplitudes of the parallel and perpendicular electric field components, respectively, δ_c is the phase shift caused by cylinder scattering. Note that Eqs. (7) and (8) are valid in the case of the normal incident and backscattering.

Equations (7) and (8) show that from measured scattering Mueller matrix it is possible to derive the size distribution and the density about the collagenous fibers (for example).

6. Conclusion

In this work, we report a PS-FFOCT system. The Mueller matrix of the system is presented. It is shown that in order to correctly interpret the measured phase retardance, the phase retardation induced by the scattering of collagenous fiber bundles at the sample surface must be removed. The initial *en-face* birefringent images of *in vitro* beef tendon samples are presented to demonstrate the power of our method. The method reported in this work is applicable to other types of PS-OCT techniques and it is also useful for deriving information about the collagenous fibers from measured birefringence.

Conflict of Interest

The authors declare no conflicts of interest.

Acknowledgments

This research was supported by the Fundamental Research Funds for the Central Universities (30920010003), and the Natural Science Foundation of China (NSFC) (61275198, 60978069).

References

1. W. Gao, "Coupling effects between dichroism and birefringence of anisotropic media," *Phys. Lett. A* **384**, 126699 (2020).
2. R. M. A. Azzam, "Propagation of partially polarized light through anisotropic media with or without depolarization: A differential 4×4 matrix calculus," *J. Opt. Soc. Am.* **68**, 1756–1767 (1978).
3. C. Fan, G. Yao, "Mapping local optical axis in birefringent samples using polarization sensitive optical coherence tomography," *J. Biomed. Opt.* **17**, 110501 (2012).
4. S. Guo, J. Zhang, L. Wang, J. S. Nelson, Z. Chen, "Depth-resolved birefringence and differential optical axis orientation measurements with fiber-based polarization-sensitive optical coherence tomography," *Opt. Lett.* **29**, 2025 (2004).
5. C. Fan, G. Yao, "Mapping local retardance in birefringent samples using polarization sensitive optical coherence tomography," *Opt. Lett.* **37**, 1415–1417 (2012).
6. S. Makita, M. Yamanari, Y. Yasuno, "Generalized Jones matrix optical coherence tomography:

Performance and local birefringence imaging," *Opt. Express* **18**, 854–876 (2010).
7. B. Braaf, K. A. Vermeer, M. de Groot, K. V. Vienola, J. F. de Boer, "Fiber-based polarization-sensitive OCT of the human retina with correction of system polarization distortions," *Biomed. Opt. Express* **5**, 2736–2758 (2014).
8. M. J. Ju, Y. J. Hong, S. Makita, Y. Lim, K. Kurokawa, L. Duan, M. Miura, S. Tang, Y. Yasuno, "Advanced multi-contrast Jones matrix optical coherence tomography for Doppler and polarization sensitive imaging," *Opt. Express* **21**, 19412–19436 (2013).
9. M. Villiger, D. Lorenser, R. A. McLaughlin, B. C. Quirk, R. W. Kirk, B. E. Bouma, D. D. Sampson, "Deep tissue volume imaging of birefringence through fibre-optic needle probes for the delineation of breast tumour," *Scientif. Rep.* **6**, 28771 (2016).
10. E. Götzinger, M. Pircher, B. Baumann, C. Hirn, C. Vass, C. K. Hitzenberger, "Retinal nerve fiber layer birefringence evaluated with polarization sensitive spectral domain OCT and scanning laser polarimetry: A comparison," *J. Biophoton.* **1**, 129–139 (2008).
11. C. Fan, G. Yao, "Imaging myocardial fiber orientation using polarization sensitive optical coherence tomography," *Biomed. Opt. Express* **4**, 460–465 (2013).
12. O. K. Naoun, V. L. Dorr, P. Allé, J.-C. Sablon, A.-M. Benoit, "Exploration of the retinal nerve fiber layer thickness by measurement of the linear dichroism," *Appl. Opt.* **44**, 7074–7082 (2005).
13. M. H. Smith, "Interpreting Mueller matrix images of tissues," *Proc. SPIE* **4257**, 82–89 (2001).
14. G. Yao, L. V. Wang, "Two-dimensional depth-resolved Mueller matrix characterization of biological tissue by optical coherence tomography," *Opt. Lett.* **24**, 537–539 (1999).
15. M. Todorović, S. Jiao, L. V. Wang, G. Stoica, "Determination of local polarization properties of biological samples in the presence of diattenuation by use of Mueller optical coherence tomography," *Opt. Lett.* **29**, 2402–2404 (2004).
16. E. Beaureparie, A. C. Boccara, M. Lebec, L. Blanchot, H. Saint-James, "Full field optical coherence microscopy," *Opt. Lett.* **23**, 244–246 (1998).
17. A. Dubois, K. Grieve, G. Moneron, R. Lecaque, L. Vabre, C. Boccara, "Ultrahigh-resolution full-field optical coherence tomography," *Appl. Opt.* **43**, 2874–2883 (2004).
18. W. Gao, "Fourier spectrum analysis of full-field optical coherence tomography for tissue imaging," *Proc. R. Soc. A* **471** (2179), 20150099 (2015).
19. W. Gao, Y. Zhu, "Fractal analysis of en face tomographic images obtained with full field optical coherence tomography," *Ann. der Phys.* **529**, 1600216 (2017).
20. G. Moneron, A. C. Boccara, A. Dubois, "Polarization-sensitive full-field optical coherence tomography," *Opt. Lett.* **32**, 2058–2060 (2007).
21. J. Moreau, V. Loriette, A. C. Boccara, "Full-field birefringence imaging by thermal-light polarization-sensitive optical coherence tomography. II. Instrument and results," *Appl. Opt.* **42**, 3811–3818 (2003).
22. J. Moreau, V. Loriette, A. C. Boccara, "Full-field birefringence imaging by thermal-light polarization-sensitive optical coherence tomography. I. Theory," *Appl. Opt.* **42**, 3800–3810 (2003).
23. S. Liu, W. Gao, "Depth-resolved imaging of intercellular structures of large intestine with polarization-sensitive FFOCT," *Opt. Lasers Eng.* **137**, 106395 (2020).
24. X. R. Huang, R. W. Knighton, "Theoretical model of the polarization properties of the retinal nerve fiber layer in reflection," *Appl. Opt.* **42**, 5726–5736 (2003).
25. C. F. Bohren, D. R. Huffman, *Absorption and Scattering of Light by Small Particles* (Wiley, New York, 1983).
26. A. M. Benoit, K. Naoun, V. Louis-Dorr, L. Mala, A. Raspiller, "Linear dichroism of the retinal nerve fiber layer expressed with Mueller matrices," *Appl. Opt.* **40**, 565–569 (2001).
27. B. H. Park, M. C. Pierce, B. Cense, J. F. de Boer, "Jones matrix analysis for a polarization-sensitive optical coherence tomography system using fiber-optic components," *Opt. Lett.* **29**, 2512–2514 (2004).
28. Y. Chang, W. Gao, "Method of interpreting Mueller matrix of anisotropic medium," *Opt. Express* **27**, 3305–3323 (2019).
29. M. Todorovic, S. Jiao, L. V. Wang, G. Stoica, "Determination of local polarization properties of biological samples in the presence of diattenuation by use of Mueller optical coherence tomography," *Opt. Lett.* **29**, 2402–2404 (2004).
30. M. K. Swami, S. Manhas, P. Buddhiwant, N. Ghosh, A. Uppal, P. K. Gupta, "Polar decomposition of 3×3 Mueller matrix: A tool for quantitative tissue polarimetry," *Opt. Express* **14**, 9324–9337 (2006).
31. N. Ortega-Quijano, T. Marvdashti, A. K. Ellerbee Bowden, "Enhanced depolarization contrast in polarization-sensitive optical coherence tomography," *Opt. Lett.* **41**, 2350–2353 (2016).
32. C. Brosseau, *Fundamentals of Polarized Light, a Statistical Approach* (John Wiley & Sons, Inc., New York, 1998).